Engineering Analysis with Boundary Elements 84 (2017) 129–140

Contents lists available at ScienceDirect

Engineering Analysis with Boundary Elements

journal homepage: www.elsevier.com/locate/enganabound

Numerical analysis of an advective diffusion domain coupled with a diffusive heat source

Roberto Pettres[a,*], Luiz Alkimin de Lacerda[a,b]

[a] UFPR – Federal University of Paraná, Postgraduate Program in Numerical Methods in Engineering. Curitiba, Paraná, Brazil
[b] Institute of Technology for Development LACTEC, Civil Structures Department DPEC, Curitiba, Paraná, CEP: 81531-090. P. O. Box: 19067 Brazil

ARTICLE INFO

Keywords:
Boundary element method
Diffusion–advective equation
Time independent fundamental solution

ABSTRACT

This paper presents a formulation of the boundary element method (BEM) for the study of heat diffusion and advective effect in isotropic and homogeneous media. The proposed formulation has a time independent fundamental solution obtained from the two-dimensional Laplace equation. Consequently, the formulation is called D-BEM since it has domain integrals in the basic integral equation. The first order time derivative that appears in the integral equations is approximated by a backward finite difference scheme. Homogeneous subregions are considered in the analysis in a specific model simulating a nonuniform flow passing by a circular obstacle under internal heat generation. Results from numerical models are compared with the available analytical solutions. The correlation estimator R^2 is employed to validate the numerical model and to demonstrate the accuracy of the proposed formulation.

1. Introduction

In engineering it is common to apply numerical methods for solving complex real problems governed by differential equations. By using appropriate models, parametric analyses allow understanding the problem under several different conditions by simply changing the model parameters. It is a cost effective approach if compared to experimental modeling.

The boundary element method (BEM) is known to be a powerful numerical technique formulated from integral equations for solving various computational mechanics problems [1,2]. It has been used to address an increasing number of problems in solid mechanics [2], fluid dynamics and acoustics [3,4], electromagnetic imaging [5], cathodic protection [6], elastodynamics [7], among others. Also, in many cases, coupled to other numerical methods [8–10]. A thorough historical review was presented by Cheng and Cheng [11].

Concerning the topic of this paper, current literature shows numerous works involving the BEM for the solution of advection and diffusion problems. Among them, Jesus and Azevedo [8], Jesus and Pereira [12] and Vanzuit [9]. In [8,9] are present solutions for the dynamic problem of heat diffusion, adopting an independent fundamental solution time marching schemes in time based on finite differences, beyond using the Houbolt method in this first work and the Hammer method in the second work with the use of cells to approximate the domain integrals, and also. In [12] is present a two-dimensional flow analysis in porous media using continuous homogeneous subregions in a stationary case based on the Laplace equation.

In [13] a BEM formulation is presented using time independent fundamental solution for the advection–diffusion steady state analysis. For the transient analyses the authors used a time dependent fundamental solution. DeSilva et al. [14] proposed solutions for the two dimensional advection–diffusion problems with variable velocities, using a time dependent fundamental solution and cell domain integrations.

Also with the use of cell integration, Lima Jr. et al. [15] numerically analyzed the mechanical behavior of continuous and saturated porous media with an implicit BEM formulation, with a time independent fundamental solution. In this work, the authors suggested a fluid structure interaction formulation, adopting, a numerical Gauss integration procedure on the boundary elements and a semi-analytical scheme for the domain cells. Other transient heat diffusion problems have also been also analyzed by others [16–18], with time dependent fundamental solutions.

Loeffler and Costalonga [19] used dual reciprocity to solve diffusive–advective problems, varying the velocity of flow and analyzing the impact on energy transport on the thermal diffusion. Also using reciprocity, Ochiai [20] presented a two-dimensional analysis of unsteady heat diffusion using a time independent BEM formulation and heat generation. In this work the author shows that it is possible to obtain satisfactory temperature distributions with the use of low order fundamental solutions. Guo et al. [21] presented a formulation to solve three-dimensional

* Corresponding author.
E-mail addresses: pettres@ufpr.br (R. Pettres), alkimin@lactec.org.br (L.A. de Lacerda).

http://dx.doi.org/10.1016/j.enganabound.2017.08.012
Received 31 January 2017; Received in revised form 16 August 2017; Accepted 16 August 2017
0955-7997/

conduction problems with transient heat generation. In their work, the time dependence on the problem was temporarily removed from the equations by Laplace transform, preserving the boundary integral equation and avoiding the domain discretization. The use of reciprocity was also observed in the work of Tanaka et al. [22], which showed a BEM approach for two-dimensional conduction problems of transient heat transfer in anisotropic media. Their work made use of a time independent fundamental solution for isotropic materials and time marching scheme based on finite differences.

A formulation of an alternative boundary element method based on an exponential transformation variable to stabilize diffusion–advection problems is presented in [23], converting the equation of diffusion–advection into a modified Helmholtz equation. In this paper the authors discuss three transformations and differentiate its use for problems dominated by diffusion and advection.

Analyses of transient heat conduction problems without domain discretization were presented by Sutradhar and Paulino [24], transforming an inhomogeneous problem in a homogeneous diffusion problem with the Laplace transform and Galerkin approximations. In this work the time dependence is restored by numerical inversion of Laplace transformation through Stehfest algorithm [25]. The results obtained with the adopted formulation were compared with the solutions obtained from finite element simulations. In [26] the method of separation of variables and the principle of Duhamel is used to transform the one-dimensional problem of diffusion and heat generation in a reverse analysis problem based on the BEM.

Transient heat conduction problems using radial integration in the BEM formulation was analyzed by Yu et al. [27].

In this analysis the authors solved the problem of heat conduction with variable thermal conductivities.

In all cited studies, the BEM is used to obtain an approximate solution of the problem and the coupling with other methods (e.g. finite difference) is a common practice. In this work, the numerical study is focused on the problem of heat diffusion and advection. Two dimensional BEM formulations with time independent fundamental solutions are coupled to solve a problem of a circular diffusive heat generating source within an advective diffusion domain. Numerical results are compared to analytical ones to validate the developed codes.

2. Mathematical model

The advective–diffusion equation in a two dimensional isotropic and homogeneous domain Ω with boundary Γ is written as [28]

$$\frac{\partial u(X,t)}{\partial t} = -\nabla \bullet [\mathbf{v}(X)\,u(X,t)] + \frac{1}{Pe}\nabla^2 u(X,t) \qquad X \in \Omega,\ X=(x,y) \tag{1}$$

where Pe is the Peclét number, defined as

$$Pe = |\,\mathbf{v}\,|\frac{B}{\alpha} \tag{2}$$

in which $\mathbf{v}$ is the velocity vector (m/s), B is the characteristic length (m), α represents the coefficient of thermal diffusivity measured in m^2/s, u is the temperature, X is the field point coordinate and t is the time variable.

The essential and natural boundary conditions are, respectively:

$$u(X,t) = \hat{u}(X,t) \quad X \in \Gamma_u \tag{3}$$

$$q(X,t) = \frac{\partial u(X,t)}{\partial n(X)} = \hat{q}(X,t) \quad X \in \Gamma_q \tag{4}$$

and the initial condition at $t = t_0$ is given by

$$u(X,t) = u_0(X,t_0) \quad X \in \Omega \tag{5}$$

3. D-BEM formulation

3.1. Advection–diffusion equation

The integral equation of the D-BEM formulation for the advective–diffusion equation can be written as follows [28]

$$\begin{aligned} C(\xi)u(\xi,t) = &\int_\Gamma u*(\xi,X)\,q(X,t)\,d\Gamma - \int_\Gamma q*(\xi,X)\,u(X,t)\,d\Gamma \\ &-Pe\int_\Omega \frac{\partial u(X,t)}{\partial t}\,u*(\xi,X)\,d\Omega \\ &-Pe\int_\Omega \nabla\bullet[\mathbf{v}(X)\,u(X,t)]\,u*(\xi,X)\,d\Omega \\ &X\in\Omega,\ X=(x,y) \end{aligned} \tag{6}$$

where $C(\xi)$ is a geometric coefficient at the collocation point ξ, q is the thermal flux and u^* and q^* are the fundamental solution and its normal derivative, respectively. The term $\mathbf{v}(X)$ represents the time independent velocity field.

The fundamental solution $u^*(\xi, X)$ in the D-BEM formulation is independent of the time variable and is given by [29],

$$u*(\xi,X) = \frac{1}{2\pi}\ln\left(\frac{1}{r}\right) \tag{7}$$

where $r = |X-\xi|$ is the distance between field and collocation points.

The derivative of the fundamental solution with respect to the normal direction to the boundary is given by

$$q*(\xi,X) = \frac{\partial u*}{\partial r}\frac{dr}{dn} = -\frac{1}{2\pi r}\frac{dr}{dn} \tag{8}$$

where n is the outward direction normal to the boundary.

The kinetic term, $\nabla\bullet[\mathbf{v}(X)\,u(X,\,t)]$, in the domain integral of Eq. (6) can be written as

$$\nabla\bullet[\mathbf{v}(X)\,u(X,t)] = \mathbf{v}(X)\bullet\nabla u(X,t) + u(X,t)\,\nabla\bullet\mathbf{v}(X) \tag{9}$$

The first term in the right side of Eq. (9) represents the thermal gradient due to transport fluid mass with velocity $\mathbf{v}$ and the second term is the temperature established by the velocity gradient. Thus, the integral containing $\nabla\bullet[\mathbf{v}(X)\,u(X,\,t)]$ takes the following form

$$\begin{aligned} \int_\Omega \nabla\bullet[\mathbf{v}(X)\,u(X,t)]\,u*(\xi,X)\,d\Omega = &\int_\Omega \mathbf{v}(X)\bullet\nabla u(X,t)\,u*(\xi,X)\,d\Omega \\ &+\int_\Omega u(X,t)\,\nabla\bullet\mathbf{v}(X)\,u*(\xi,X)\,d\Omega \end{aligned} \tag{10}$$

For simplicity, the time derivative presented in Eq. (6) is approximated by the backward finite difference formula [30]

$$\frac{\partial u(X,t)}{\partial t} = \frac{u(X,t+\Delta t)-u(X,t)}{\Delta t} \tag{11}$$

Replacing Eqs. (10) and (11) in Eq. (6) and grouping terms conveniently, one has

$$\begin{aligned} C(\xi)u(\xi,t+\Delta t) = &\int_\Gamma u*(\xi,X)\,q(X,t+\Delta t)\,d\Gamma - \int_\Gamma q*(\xi,X)\,u(X,t+\Delta t)\,d\Gamma \\ &-Pe\left[\int_\Omega \mathbf{v}(X)\bullet\nabla u(X,t+\Delta t)\,u*(\xi,X)\,d\Omega \right. \\ &\left.+\int_\Omega u(X,t+\Delta t)\,\nabla\bullet\mathbf{v}(X)\,u*(\xi,X)\,d\Omega\right] \\ &-\frac{Pe}{\Delta t}\left[\int_\Omega u(X,t+\Delta t)\,u*(\xi,X)\,d\Omega - \int_\Omega u(X,t)\,u*(\xi,X)\,d\Omega\right] \\ &X\in\Omega,\ X=(x,y) \end{aligned} \tag{12}$$

Eq. (12) can be used recursively for the solution of advective–diffusion problems, starting with known variables at time t_τ and determining the unknown variables at time $t_{\tau+1}$. According to [31], the time step, Δt_c, can be estimated as

$$\Delta t_c \le \frac{{L_j}^2}{2\alpha} \tag{13}$$

where L_j is the boundary element size.

For a general problem solution, the boundary is divided into n boundary elements, approximating the geometry of each element with linear interpolation functions. Within each element the potential and flux variables are approximated by linear continuous functions. The domain is dicretized in m cells assuming a constant behavior of the potential within each cell [32].

Discretization of the domain integrals containing the kinetic terms gives

$$\int_\Omega \mathbf{v}(X)\bullet\nabla u(X,t)\,u*(\xi,X)\,d\Omega+\int_\Omega u(X,t)\,\nabla\bullet\mathbf{v}(X)\,u*(\xi,X)\,d\Omega$$
$$=\sum_{d=1}^{m}\int_\Omega \mathbf{v}(X)\bullet\nabla u(X,t)\,u*(\xi,X)\,d\Omega$$
$$+\sum_{d=1}^{m}\int_\Omega u(X,t)\,\nabla\bullet\mathbf{v}(X)\,u*(\xi,X)\,d\Omega \tag{14}$$

Assuming that the velocity field is known and that the temperature within each cell is constant, the calculation of the first integral on the right side of Eq. (14) takes the following form:

$$\sum_{d=1}^{m}\int_\Omega \mathbf{v}(X)\bullet\nabla\, u(X,t)\,u*(\xi,X)\,d\Omega=\sum_{d=1}^{m}\mathbf{v}(X)\int_\Omega\nabla u(X,t)\,u*(\xi,X)\,d\Omega \tag{15}$$

which can be expanded to:

$$\sum_{d=1}^{m}\mathbf{v}(X)\int_\Omega\nabla u(X,t)\,u*(\xi,X)\,d\Omega=\sum_{d=1}^{m}v_x(X)\int_\Omega\frac{\partial u(X,t)}{\partial x}\,u*(\xi,X)\,d\Omega$$
$$+\sum_{d=1}^{m}v_y(X)\int_\Omega\frac{\partial u(X,t)}{\partial y}\,u*(\xi,X)\,d\Omega \tag{16}$$

Integrating by parts each integral on the right hand side of Eq. (16), one obtains:

$$\sum_{d=1}^{m}v_x(X)\int_{\Omega_d}\frac{\partial u(X,t)}{\partial x}\,u*(\xi,X)\,d\Omega$$
$$=\sum_{b=1}^{n}v_x(X)\int_\Gamma u(X,t)\,\eta\frac{1}{2\pi}\ln\left(\frac{1}{r}\right)d\Gamma$$
$$+\sum_{d=1}^{m}v_x(X)\int_\Omega u(X,t)\frac{1}{2\pi r\cos(\theta)}\,d\Omega$$
$$\sum_{d=1}^{m}v_y(X)\int_\Omega\frac{\partial u(X,t)}{\partial y}\,u*(\xi,X)\,d\Omega$$
$$=\sum_{b=1}^{n}v_y(X)\int_\Gamma u(X,t)\,\eta\frac{1}{2\pi}\ln\left(\frac{1}{r}\right)d\Gamma$$
$$+\sum_{d=1}^{m}v_y(X)\int_\Omega u(X,t)\frac{1}{2\pi r\sin(\theta)}\,d\Omega \tag{17}$$

where η is the normal vector component at the boundary and θ represents the angle between the vector $\boldsymbol{r}$ and its x component. Substituting the field variables by the adopted approximating functions, results:

$$\sum_{d=1}^{m}v_x(X)\int_\Omega\frac{\partial u(X,t)}{\partial x}\,u*(\xi,X)\,d\Omega$$
$$=\sum_{b=1}^{n}v_x(X)\int_\Gamma\eta\frac{1}{2\pi}\ln\left(\frac{1}{r}\right)\begin{bmatrix}\varphi_1 & \varphi_2\end{bmatrix}d\Gamma\begin{Bmatrix}u_1\\u_2\end{Bmatrix}$$
$$+\sum_{d=1}^{m}v_x(X)\,u(X,t)\int_\Omega\frac{1}{2\pi r\cos(\theta)}\,d\Omega$$
$$\sum_{d=1}^{m}v_y(X)\int_\Omega\frac{\partial u(X,t)}{\partial y}\,u*(\xi,X)\,d\Omega$$
$$=\sum_{b=1}^{n}v_y(X)\int_\Gamma\eta\frac{1}{2\pi}\ln\left(\frac{1}{r}\right)\begin{bmatrix}\varphi_1 & \varphi_2\end{bmatrix}d\Gamma\begin{Bmatrix}u_1\\u_2\end{Bmatrix}$$
$$+\sum_{d=1}^{m}v_y(X)\,u(X,t)\int_\Omega\frac{1}{2\pi r\sin(\theta)}\,d\Omega \tag{18}$$

Also, the second integral on the right hand side of Eq. (14) takes the following form:

$$\sum_{d=1}^{m}\int_\Omega u(X,t)\,\nabla\bullet\mathbf{v}(X)\,u*(\xi,X)\,d\Omega=\sum_{d=1}^{m}u(X,t)\int_\Omega\nabla\bullet\mathbf{v}(X)u*(\xi,X)\,d\Omega \tag{19}$$

which can be expanded to:

$$\sum_{d=1}^{m}u(X,t)\int_\Omega\nabla\bullet\mathbf{v}(X)\,u*(\xi,X)\,d\Omega=\sum_{d=1}^{m}u(X,t)\int_\Omega\frac{\partial v_x(X)}{\partial x}\,u*(\xi,X)\,d\Omega$$
$$+\sum_{d=1}^{m}u(X,t)\int_\Omega\frac{\partial v_y(X)}{\partial y}\,u*(\xi,X)\,d\Omega \tag{20}$$

Integrating by parts, in an analogous procedure to that of the Eq. (15), and substituting the field variables approximations, one obtains:

$$\int_\Omega \mathbf{v}(X)\bullet\nabla u(X,t)\,u*(\xi,X)\,d\Omega+\int_\Omega u(X,t)\,\nabla\bullet\mathbf{v}(X)\,u*(\xi,X)\,d\Omega$$
$$=\sum_{b=1}^{n}v_x(X)\int_\Gamma\eta\frac{1}{\pi}\ln\left(\frac{1}{r}\right)\begin{bmatrix}\varphi_1 & \varphi_2\end{bmatrix}d\Gamma\begin{Bmatrix}u_1\\u_2\end{Bmatrix}$$
$$+\sum_{d=1}^{m}v_x(X)\,u(X,t)\int_\Omega\frac{1}{\pi r\cos(\theta)}\,d\Omega$$
$$+\sum_{b=1}^{n}v_y(X)\int_\Gamma\eta\frac{1}{\pi}\ln\left(\frac{1}{r}\right)\begin{bmatrix}\varphi_1 & \varphi_2\end{bmatrix}d\Gamma\begin{Bmatrix}u_1\\u_2\end{Bmatrix}$$
$$+\sum_{d=1}^{m}v_y(X)\,u(X,t)\int_\Omega\frac{1}{\pi r\sin(\theta)}\,d\Omega \tag{21}$$

Applying Eq. (12) to all boundary nodes and internal points, the following system of equations is obtained:

$$\begin{bmatrix}\mathbf{H}^{bb}+\mathbf{V}^{bb} & \frac{1}{\alpha\Delta t}\mathbf{M}^{bd}+\mathbf{W}^{bd}\\ \mathbf{H}^{db}+\mathbf{W}^{db} & \mathbf{I}+\frac{1}{\alpha\Delta t}\mathbf{M}^{dd}+\mathbf{W}^{dd}\end{bmatrix}\begin{bmatrix}\mathbf{u}^b\\\mathbf{u}^d\end{bmatrix}_{\tau+1}$$
$$=\begin{bmatrix}\mathbf{G}^{bb}\\\mathbf{G}^{db}\end{bmatrix}[\mathbf{q}^b]_{\tau+1}+\frac{1}{\alpha\Delta t}\begin{bmatrix}\mathbf{M}^{bd}\\\mathbf{M}^{dd}\end{bmatrix}[\mathbf{u}^d]_\tau \tag{22}$$

where **H, G** and **V** are submatrices which result from the boundary integrals; the submatrices **M** and **W** result from the domain integrals and **I** is an identity submatrix. The first superindex indicates the position of the collocation point and the second one the position of the field point, with b meaning boundary and d meaning domain. The subindex $\tau+1$ indicates the time $t_{\tau+1}=(\tau+1)\Delta t$ and the subindex τ the time $t_\tau=\tau\Delta t$. In this work a constant value is assumed for the timestep Δt, estimated according to Eq. (13).

After imposing the initial and boundary conditions, the system of Eq. (22) is solved and the unknown potential and flux values at the boundary nodes and potential values at the internal points are determined at the time $t_{\tau+1}$. The potential values are updated and the problem solution continues, recursively.

In general, after imposing the boundary conditions, one has

$$\mathbf{A}\,x^{\tau+1}=y^{\tau+1}+y^\tau \tag{23}$$

where $\tau\geq 0$ and

- $x^{\tau+1}$ is the vector of unknown nodal values at time $t_{\tau+1}$;
- **A** is the coefficient matrix that contains terms relating to **H, G, V, W** and **M**;
- $y^{\tau+1}$ is a vector that represents contribution from the known values at the time $t_{\tau+1}$, and y^τ the contribution from the previous time t_τ.

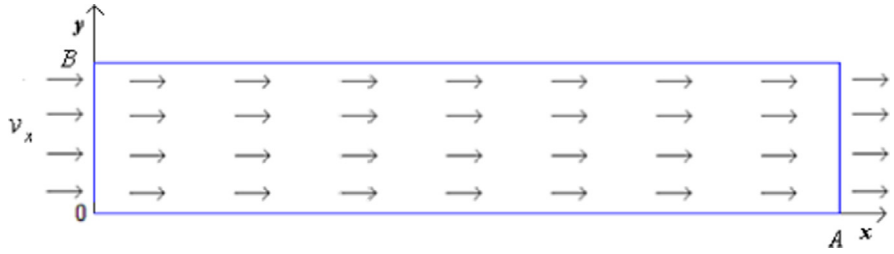

Fig. 1. Rectangular domain under uniform flow with velocity v.

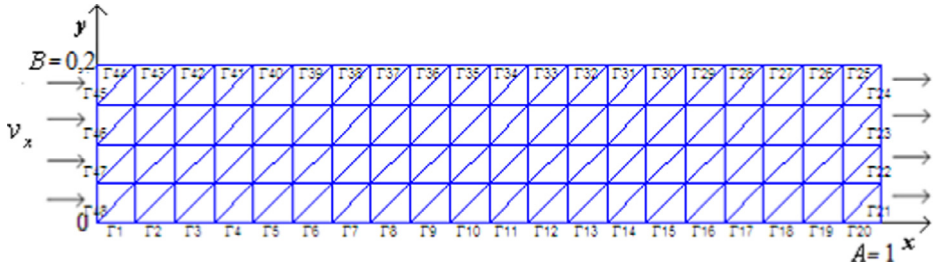

Fig. 2. Domain discretization with 160 triangular cells.

Comment on the singular integrations—same as in the classical 2d BEM formulation. To calculate the integral domain, the integration based on triangular cells with constant variations was used. For more details, see [32]. Singular integration algorithms where implementation according to [32].

This D-BEM formulation was implemented in the software Matlab 7.0-R2009.

3.2. Example – rectangular domain with uniform flow velocity

In the first numerical example a rectangular area (A × B in mm) is subjected to a laminar uniform flow along the x direction, as shown in Fig. 1. The constant velocity field components are

$$\begin{aligned} v_x &= v \\ v_y &= 0 \end{aligned} \tag{24}$$

The rectangular domain has dimensions $A = 1$ and $B = 0.2$ (Fig. 2), which was discretized with 160 triangular cells and 48 linear boundary elements.

3.2.1. Constant boundary conditions

The first evaluation was performed considering the following constant boundary conditions:

$$\begin{aligned} u(0, y, t) &= 1°\mathrm{C} \\ u(A, y, t) &= 0°\mathrm{C} \\ q(x, 0, t) &= 0\mathrm{W/mm}^2 \\ q(x, B, t) &= 0\mathrm{W/mm}^2 \end{aligned} \tag{25}$$

with the initial condition:

$$u_0(x, y, t_0) = 0°\mathrm{C} \tag{26}$$

The analytical solution of this problem is given by [14]:

$$u(x, y, t) = \frac{\exp(Pe\, x) - \exp(Pe)}{1 - \exp(Pe)} - 2\sum_{n=1}^{\infty} \frac{n\pi}{\lambda_n} \exp\left(\frac{Pe\, x}{2} - \lambda_n t\right) \sin(n\pi x) \tag{27}$$

with

$$\lambda_n = n^2\pi^2 + \left(\frac{Pe}{2}\right)^2$$

The numerical solution of the problem is compared to the analytical one considering $v_x = 0.001$ mm/s and $\alpha = 1.0$ mm^2/s. Temperature results at the center of the rectangular domain are shown in Fig. 3. An excellent agreement between numerical and analytical results is observed.

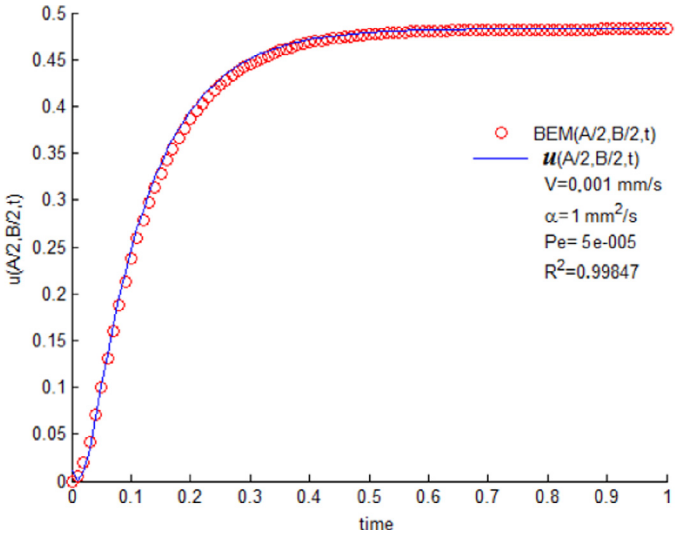

Fig. 3. Comparison of the analytical and the D-BEM solutions at the center point of domain with $\alpha = 1.0$ mm^2/s and $v_x = 0.001$ mm/s.

The same problem was analyzed for different flow velocity values with v_x equal to 0.0, 0.001, 0.005 and 0.010 mm/s and the R^2 correlation between analytical and numerical results were 0.99890, 0.99847, 0.99808 and 0.99589, respectively.

Fig. 4 shows the numerical temperature evolution at the center point of the domain for different flow velocities. Differences are not significant (near 2.0%) in the range of tested values. Only at a closer view differences can be clearly noticed.

3.2.2. Time dependent boundary conditions

A second evaluation was performed with the following time-dependent boundary conditions, which were applied to the left and right sides of the domain, respectively:

$$\begin{aligned} u(0, y, t) &= \frac{1}{\sqrt{4t+1}} \exp\left[-\frac{(-1 - v_x t)^2}{\alpha(4t+1)}\right]^{\circ} C \\ u(A, y, t) &= \frac{1}{\sqrt{4t+1}} \exp\left[-\frac{(-v_x t)^2}{\alpha(4t+1)}\right]^{\circ} C \end{aligned} \tag{28}$$

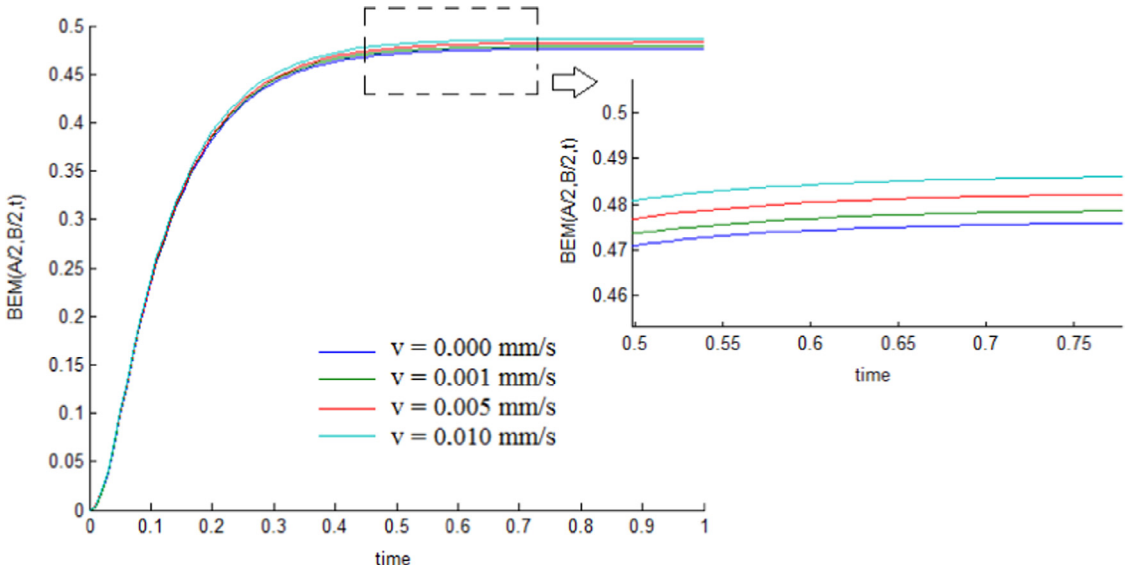

Fig. 4. Comparison of the BEM solution to different velocities.

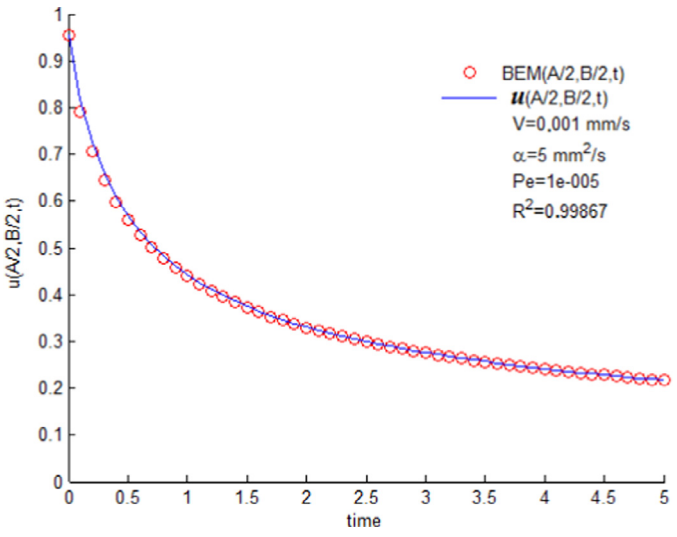

Fig. 5. Comparison of the analytical and D-BEM solutions at the center point of domain with $\alpha = 5.0\ \text{mm}^2/\text{s}$ and $v_x = 0.001$ mm/s.

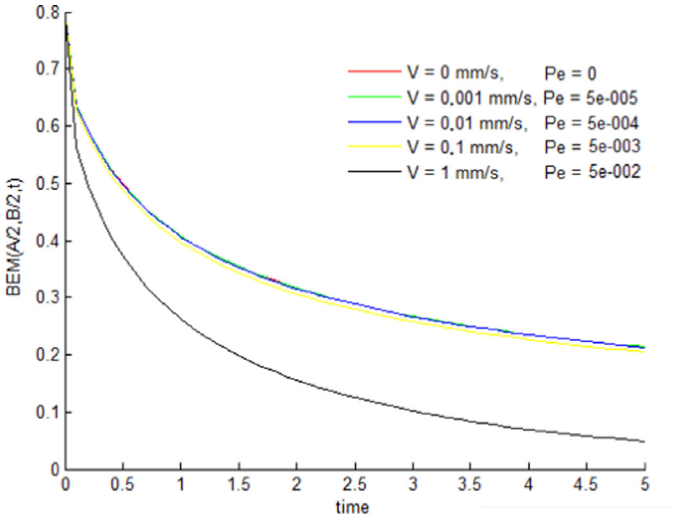

Fig. 6. D-BEM solutions for temperature at the center point of domain with $\alpha = 1.0\ \text{mm}^2/\text{s}$.

with zero normal flux through the upper and bottom sides of the domain,

$$q(x,0,t) = 0\,\text{W/mm}^2 \qquad q(x,B,t) = 0\,\text{W/mm}^2 \tag{29}$$

The initial condition is given by:

$$u_0(X,t_0) = \exp\left(\frac{-x^2}{\alpha}\right)^{\circ} C \quad X \in \Omega \tag{30}$$

The analytical solution for this problem is known and is given by [33]:

$$u(x,y,t) = \frac{1}{\sqrt{4t+1}} \exp\left(-\frac{(x-1-v_x t)^2}{\alpha(4t+1)}\right) \tag{31}$$

The numerical solution of the problem is compared to the analytical one considering $v_x = 0.001$ mm/s and $\alpha = 5.0\text{mm}^2/\text{s}$. Temperature results at the center of the rectangular domain are shown in Fig. 5, where an excellent agreement between numerical and analytical data is observed.

The same problem was analyzed for different values of thermal diffusivity: 0.5, 5.0, 10.0, 50.0 and 100.0 mm^2/s and the mean R^2 correlations between analytical and numerical results for all cells were 0.964402, 0.999278, 0.999811, 0.999992, and 0.999998, respectively. The correlation is clearly improving with the reducing Peclét number.

A similar evaluation was performed by keeping thermal diffusivity equal to 1.0 mm^2/s and changing the flow velocity v_x with values 0.0, 0.001, 0.01, 0.1 and 1.0 mm/s. The corresponding R^2 correlations were 0.987115, 0.987096, 0.986927, 0.985361, and 0.985042, respectively. In this case, the correlation is slowly and progressively reducing since the size of the boundary elements were kept the same, increasing the Peclét number.

Fig. 6 shows the numerical temperature evolution at the center point of the domain for the different flow velocities. Differences are not significant (less than 2.5%) in the range of tested values between 0 and 0.1 mm/s. Only at a closer view (see Fig. 7) differences can be noticed.

3.3. Diffusion equation with heat source

Let Ω_2 be an isotropic domain containing a non-homogeneous internal heat source $F(X, t)$. The governing diffusion equation is

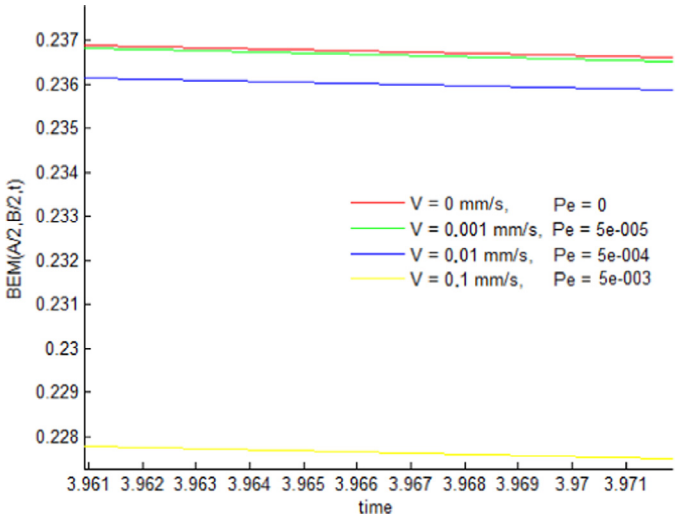

Fig. 7. Closer view of D-BEM solutions for temperature at the center point of domain with $\alpha = 1.0\ \mathrm{mm^2/s}$.

given by [34]:

$$\nabla^2 u(X,t) + F(X,t) = \frac{1}{\alpha}\frac{\partial u(X,t)}{\partial t} \quad X \in \Omega_2,\ X = (x,y) \tag{32}$$

and the corresponding boundary integral equation is:

$$C(\xi)\,u(\xi,t) = \int_\Gamma u*(\xi,X)\,q(X,t)\,d\Gamma - \int_\Gamma q*(\xi,X)\,u(X,t)\,d\Gamma - \frac{1}{\alpha}\int_\Omega \frac{\partial u(X,t)}{\partial t}\,u*(\xi,X)\,d\Omega + \int_\Omega F(X,t)\,u*(\xi,X)\,d\Omega \tag{33}$$

Once again, approximating the first order time derivative in the first domain integral on the right hand side of Eq. (33), one has:

$$C(\xi)\,u(\xi,t+\Delta t) = \int_\Gamma u*(\xi,X)\,q(X,t+\Delta t)\,d\Gamma - \int_\Gamma q*(\xi,X)\,u(X,t+\Delta t)\,d\Gamma + -\frac{1}{\alpha\,\Delta t}\left(\int_\Omega u(X,t+\Delta t)\,u*(\xi,X)\,d\Omega - \int_\Omega u(X,t)\,u*(\xi,X)\,d\Omega\right) + \int_\Omega F(X,t)\,u*(\xi,X)\,d\Omega \tag{34}$$

The same linear and constant approximations may be employed for the field variables at the boundary and at the domain, respectively. Numerical integrations may be carried out as in [32].

3.4. Coupling D-BEM formulations

3.4.1. Matrix notation and numerical solution to the problem of diffusion–advection

Consider now an advection–diffusion domain Ω_1, which contains a general heat source bounded by Ω_2 (Fig. 8).

The integral Eq. (12) can be applied to all nodes of domain Ω_1, while integral Eq. (34) is valid in all nodes of Ω_2. By applying them to all nodes of each domain, the following coupled system of equation is formed:

$$\begin{bmatrix} \mathbf{H}^{bb}_{1,1} & \mathbf{H}^{bb}_{1,2} & 0 & 0 & 0 \\ \mathbf{H}^{bb}_{2,1} & \mathbf{H}^{bb}_{2,2} & 0 & 0 & 0 \\ \mathbf{H}^{db}_{1,1} & \mathbf{H}^{db}_{1,2} & \mathbf{I} & 0 & 0 \\ 0 & 0 & 0 & \mathbf{H}^{bb}_{3,3} & 0 \\ 0 & 0 & 0 & \mathbf{H}^{db}_{2,3} & \mathbf{I} \end{bmatrix} \begin{bmatrix} \mathbf{u}^b_1 \\ \mathbf{u}^b_2 \\ \mathbf{u}^d_1 \\ \mathbf{u}^b_3 \\ \mathbf{u}^d_2 \end{bmatrix}_{\tau+1} = \begin{bmatrix} \mathbf{G}^{bb}_{1,1} & \mathbf{G}^{bb}_{1,2} & 0 \\ \mathbf{G}^{bb}_{2,1} & \mathbf{G}^{bb}_{2,2} & 0 \\ \mathbf{G}^{db}_{1,1} & \mathbf{G}^{db}_{1,2} & 0 \\ 0 & 0 & \mathbf{G}^{bb}_{3,3} \\ 0 & 0 & \mathbf{G}^{db}_{2,3} \end{bmatrix} \begin{bmatrix} \mathbf{q}^b_1 \\ \mathbf{q}^b_2 \\ \mathbf{q}^b_3 \end{bmatrix}_{\tau+1} + -\frac{1}{\alpha_1\,\Delta t}\begin{bmatrix} \mathbf{M}^{bd}_{1,1} \\ \mathbf{M}^{bd}_{2,1} \\ \mathbf{M}^{dd}_{1,1} \\ 0 \\ 0 \end{bmatrix} \left\{ \left[\mathbf{u}^d_1\right]_{\tau+1} - \left[\mathbf{u}^d_1\right]_\tau \right\} + -\frac{1}{\alpha_2\,\Delta t}\begin{bmatrix} 0 \\ 0 \\ 0 \\ \mathbf{M}^{bd}_{3,2} \\ \mathbf{M}^{dd}_{2,2} \end{bmatrix} \left\{ \left[\mathbf{u}^d_2\right]_{\tau+1} - \left[\mathbf{u}^d_2\right]_\tau \right\} + -\begin{bmatrix} \mathbf{V}^{bd}_{1,1} \\ \mathbf{V}^{bd}_{2,1} \\ \mathbf{V}^{dd}_{1,1} \\ 0 \\ 0 \end{bmatrix} \left[\mathbf{u}^d_1\right]_{\tau+1} - \begin{bmatrix} \mathbf{V}^{bb}_{1,1} & \mathbf{V}^{bb}_{1,2} \\ \mathbf{V}^{bb}_{2,1} & \mathbf{V}^{bb}_{2,2} \\ \mathbf{V}^{db}_{1,1} & \mathbf{V}^{db}_{1,2} \\ 0 & 0 \\ 0 & 0 \end{bmatrix} \begin{bmatrix} \mathbf{u}^b_1 \\ \mathbf{u}^b_2 \end{bmatrix} + \frac{1}{k}\begin{bmatrix} 0 \\ 0 \\ 0 \\ \mathbf{F}^{bd}_{3,3} \\ \mathbf{F}^{dd}_{2,2} \end{bmatrix}_{\tau+1} \tag{35}$$

In the above equation, $\mathbf{V^{bd}}$, $\mathbf{V^{bc}}$ and $\mathbf{V^{dd}}$ are matrices resulting from the domain integration while $\mathbf{V^{bb}}$ results from boundary integrals. By grouping similar terms of the system of Eq. (35), one obtains:

$$\begin{bmatrix} \mathbf{H}^{bb}_{1,1}+\mathbf{V}^{bb}_{1,1} & \mathbf{H}^{bb}_{1,2}+\mathbf{V}^{bb}_{1,2} & \frac{1}{\alpha_1\Delta t}\mathbf{M}^{bd}_{1,1}+\mathbf{V}^{bd}_{1,1} & 0 & 0 \\ \mathbf{H}^{bb}_{2,1}+\mathbf{V}^{bb}_{2,1} & \mathbf{H}^{bb}_{2,2}+\mathbf{V}^{bb}_{2,2} & \frac{1}{\alpha_1\Delta t}\mathbf{M}^{bd}_{2,1}+\mathbf{V}^{bd}_{2,1} & 0 & 0 \\ \mathbf{H}^{db}_{1,1}+\mathbf{V}^{db}_{1,1} & \mathbf{H}^{db}_{1,2}+\mathbf{V}^{db}_{1,2} & \mathbf{I}+\frac{1}{\alpha_1\Delta t}\mathbf{M}^{dd}_{1,1}+\mathbf{V}^{dd}_{1,1} & 0 & 0 \\ 0 & 0 & 0 & \mathbf{H}^{bb}_{3,3} & \frac{1}{\alpha_2\Delta t}\mathbf{M}^{bd}_{3,2} \\ 0 & 0 & 0 & \mathbf{H}^{db}_{2,3} & \mathbf{I}+\frac{1}{\alpha_2\Delta t}\mathbf{M}^{dd}_{2} \end{bmatrix} \times \begin{bmatrix} \mathbf{u}^b_1 \\ \mathbf{u}^b_2 \\ \mathbf{u}^d_1 \\ \mathbf{u}^b_3 \\ \mathbf{u}^d_2 \end{bmatrix}_{\tau+1} = \begin{bmatrix} \mathbf{G}^{bb}_{1,1} & \mathbf{G}^{bb}_{1,2} & 0 \\ \mathbf{G}^{bb}_{2,1} & \mathbf{G}^{bb}_{2,2} & 0 \\ \mathbf{G}^{db}_{1,1} & \mathbf{G}^{db}_{1,2} & 0 \\ 0 & 0 & \mathbf{G}^{bb}_{3,3} \\ 0 & 0 & \mathbf{G}^{db}_{2,3} \end{bmatrix} \begin{bmatrix} \mathbf{q}^b_1 \\ \mathbf{q}^b_2 \\ \mathbf{q}^b_3 \end{bmatrix}_{\tau+1} + \frac{1}{\alpha_1\,\Delta t}\begin{bmatrix} \mathbf{M}^{bd}_{1,1} \\ \mathbf{M}^{bd}_{2,1} \\ \mathbf{M}^{dd}_{1,1} \\ 0 \\ 0 \end{bmatrix} \left[\mathbf{u}^d_1\right]_\tau + \frac{1}{\alpha_2\,\Delta t}\begin{bmatrix} 0 \\ 0 \\ 0 \\ \mathbf{M}^{bd}_{3,2} \\ \mathbf{M}^{dd}_{2,2} \end{bmatrix} \left[\mathbf{u}^d_2\right]_\tau + \frac{1}{k}\begin{bmatrix} 0 \\ 0 \\ 0 \\ \mathbf{F}^{bd}_{3,3} \\ \mathbf{F}^{dd}_{2,2} \end{bmatrix}_{\tau+1} \tag{36}$$

Transferring the column coefficients of the matrices on the right hand corresponding to the unknowns, to the left hand side of the equation, one has:

$$\begin{bmatrix} \mathbf{H}^{bb}_{1,1}+\mathbf{V}^{bb}_{1,1} & \mathbf{H}^{bb}_{1,2}+\mathbf{V}^{bb}_{1,2} & \frac{1}{\alpha_1\Delta t}\mathbf{M}^{bd}_{1,1}+\mathbf{V}^{bd}_{1,1} & 0 & 0 & -\mathbf{G}^{bb}_{1,2} & 0 \\ \mathbf{H}^{bb}_{2,1}+\mathbf{V}^{bb}_{2,1} & \mathbf{H}^{bb}_{2,2}+\mathbf{V}^{bb}_{2,2} & \frac{1}{\alpha_1\Delta t}\mathbf{M}^{bd}_{2,1}+\mathbf{V}^{bd}_{2,1} & 0 & 0 & -\mathbf{G}^{bb}_{2,2} & 0 \\ \mathbf{H}^{db}_{1,1}+\mathbf{V}^{db}_{1,1} & \mathbf{H}^{db}_{1,2}+\mathbf{V}^{db}_{1,2} & \mathbf{I}+\frac{1}{\alpha_1\Delta t}\mathbf{M}^{dd}_{1,1}+\mathbf{V}^{dd}_{1,1} & 0 & 0 & -\mathbf{G}^{db}_{1,2} & 0 \\ 0 & 0 & 0 & \mathbf{H}^{bb}_{3,3} & \frac{1}{\alpha_2\Delta t}\mathbf{M}^{bd}_{3,2} & 0 & -\mathbf{G}^{bb}_{3,3} \\ 0 & 0 & 0 & \mathbf{H}^{db}_{2,3} & \mathbf{I}+\frac{1}{\alpha_2\Delta t}\mathbf{M}^{dd}_{2} & 0 & -\mathbf{G}^{db}_{2,3} \end{bmatrix} \times \begin{bmatrix} \mathbf{u}^b_1 \\ \mathbf{u}^b_2 \\ \mathbf{u}^d_1 \\ \mathbf{u}^b_3 \\ \mathbf{u}^d_2 \\ \mathbf{q}^b_2 \\ \mathbf{q}^b_3 \end{bmatrix}_{\tau+1} = \begin{bmatrix} \mathbf{G}^{bb}_{1,1} \\ \mathbf{G}^{bb}_{2,1} \\ \mathbf{G}^{db}_{1,1} \\ 0 \\ 0 \end{bmatrix} \left[\mathbf{q}^b_1\right]_{\tau+1} + \frac{1}{\alpha_1\,\Delta t}\begin{bmatrix} \mathbf{M}^{bd}_{1,1} \\ \mathbf{M}^{bd}_{2,1} \\ \mathbf{M}^{dd}_{1,1} \\ 0 \\ 0 \end{bmatrix} \left[\mathbf{u}^d_1\right]_\tau + \frac{1}{\alpha_2\,\Delta t}\begin{bmatrix} 0 \\ 0 \\ 0 \\ \mathbf{M}^{bd}_{3,2} \\ \mathbf{M}^{dd}_{2,2} \end{bmatrix} \left[\mathbf{u}^d_2\right]_\tau + \frac{1}{k}\begin{bmatrix} 0 \\ 0 \\ 0 \\ \mathbf{F}^{bd}_{3,3} \\ \mathbf{F}^{dd}_{2,2} \end{bmatrix}_{\tau+1} \tag{37}$$

Applying the equilibrium and compatibility equations in the interface between Ω_1 and Ω_2,

$$\begin{aligned} \mathbf{u}^b_2 &= \mathbf{u}^b_3 \\ \mathbf{q}^b_2 &= -\mathbf{q}^b_3 \end{aligned} \tag{38}$$

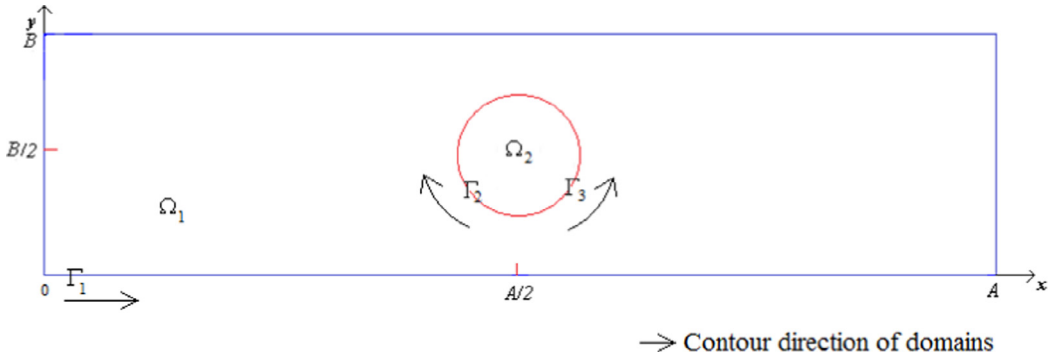

Fig. 8. Domain Ω_1 with contours Γ_1 ,Γ_2 and domain Ω_2 with contours Γ_3.

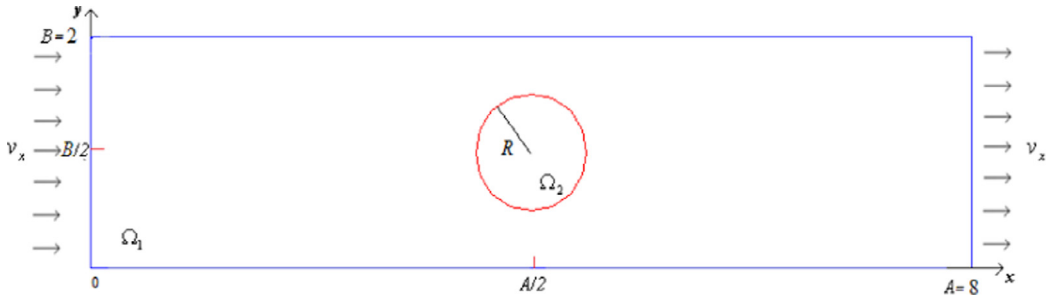

Fig. 9. Geometric model of the diffusion problem with advection and heat source.

allow reducing the number of unknowns of the system of Eq. (37) to the same number of equations:

$$\begin{bmatrix} \mathbf{H}^{bb}_{1,1}-\mathbf{V}^{bb}_{1,1} & \mathbf{H}^{bb}_{1,2}-\mathbf{V}^{bb}_{1,2} & \frac{1}{\alpha_1\Delta t}\mathbf{M}^{bd}_{1,1}-\mathbf{V}^{bd}_{1,1} & \mathbf{G}^{bb}_{1,2} & 0 \\ \mathbf{H}^{bb}_{2,1}-\mathbf{V}^{bb}_{2,1} & \mathbf{H}^{bb}_{2,2}-\mathbf{V}^{bb}_{2,2} & \frac{1}{\alpha_1\Delta t}\mathbf{M}^{bd}_{2,1}-\mathbf{V}^{bd}_{2,1} & \mathbf{G}^{bb}_{2,2} & 0 \\ \mathbf{H}^{db}_{1,1}-\mathbf{V}^{db}_{1,1} & \mathbf{H}^{db}_{1,2}-\mathbf{V}^{db}_{1,2} & \mathbf{I}+\frac{1}{\alpha_1\Delta t}\mathbf{M}^{dd}_{1,1}-\mathbf{V}^{dd}_{1,1} & \mathbf{G}^{db}_{1,2} & 0 \\ 0 & \mathbf{H}^{bb}_{3,3} & 0 & -\mathbf{G}^{bb}_{3,3} & \frac{1}{\alpha_2\Delta t}\mathbf{M}^{bd}_{3,2} \\ 0 & \mathbf{H}^{db}_{2,3} & 0 & -\mathbf{G}^{db}_{2,3} & \mathbf{I}+\frac{1}{\alpha_2\Delta t}\mathbf{M}^{dd}_{2} \end{bmatrix}$$
$$\times \begin{bmatrix} \mathbf{u}^b_1 \\ \mathbf{u}^b_2=\mathbf{u}^b_3 \\ \mathbf{u}^d_1 \\ \mathbf{q}^b_2=-\mathbf{q}^b_3 \\ \mathbf{u}^d_2 \end{bmatrix}_{\tau+1} = \begin{bmatrix} \mathbf{G}^{bb}_{1,1} \\ \mathbf{G}^{bb}_{2,1} \\ \mathbf{G}^{db}_{1,1} \\ 0 \\ 0 \end{bmatrix} [\mathbf{q}^b_1]_{\tau+1} + \frac{1}{\alpha_1\Delta t} \begin{bmatrix} \mathbf{M}^{bd}_{1,1} \\ \mathbf{M}^{bd}_{2,1} \\ \mathbf{M}^{dd}_{1,1} \\ 0 \\ 0 \end{bmatrix} [\mathbf{u}^d_1]_\tau$$
$$+ \frac{1}{\alpha_2\Delta t} \begin{bmatrix} 0 \\ 0 \\ 0 \\ \mathbf{M}^{bd}_{3,2} \\ \mathbf{M}^{dd}_{2,2} \end{bmatrix} [\mathbf{u}^d_2]_\tau + \frac{1}{k} \begin{bmatrix} 0 \\ 0 \\ 0 \\ \mathbf{F}^{cd}_{3,3} \\ \mathbf{F}^{dd}_{2,2} \end{bmatrix}_{\tau+1} \tag{39}$$

Eq. (39) can be rearranged as Eq. (23) and solved with the same time marching scheme used previously.

3.5. Example – rectangular domain with a circular heat source obstacle and a non-uniform velocity field

The numerical advection diffusion evaluation in this section refers to a channel (Ω_1, $A = 8$ and $B = 2$) subjected to a laminar irrotational flow containing a circular obstacle with a heat generation condition (Ω_2, $R = 0{,}5$). Fig. 9 illustrates the problem domains.

3.5.1. Flow around a circular obstacle – approximate velocity field

The continuity equation for a laminar flow case is given by [34]:

$$\nabla^2\Phi(X) = 0 \tag{40}$$

Eq. (40) represents a scalar velocity potential function in an irrotational flow domain. The velocity vector $\mathbf{v}(X)$ can be expressed as the gradient of this function, with:

$$\nabla\Phi(X) = \mathbf{v}(X) \tag{41}$$

The following essential conditions are adopted for the boundary Γ_1,

$$v_x = \frac{\partial\Phi(X)}{\partial x} = v; \quad v_y = \frac{\partial\Phi(X)}{\partial y} = 0 \quad X \in \Gamma_1 \tag{42}$$

representing a constant velocity along the x-axis direction and null velocity on the y-axis direction (see Fig. 10). Also, the natural boundary condition

$$\Lambda(X) = \frac{\partial\Phi(X)}{\partial n(X)} = 0 \quad X \in \Gamma_2 \tag{43}$$

is considered in the boundary of the rigid obstacle, representing null velocity in the normal direction to Γ_2.

The approximate velocity field in polar coordinates, with the versors $\hat{\mathbf{i}}$ and $\hat{\mathbf{j}}$ in the directions r and θ, is given by [35]:

$$\mathbf{v}(X) = \vartheta\hat{\mathbf{i}} + \nu\hat{\mathbf{j}} \tag{44}$$

where the variables ϑ and ν are given by:

$$\vartheta(r,\theta) = v_x\left[1 - \frac{R^2\cos(2\theta)}{r^2}\right] \tag{45}$$

$$\nu(r,\theta) = -v_x\frac{R^2\sin(2\theta)}{r^2} \tag{46}$$

where R is radius of circular obstacle (domain Ω_2).

3.5.2. Geometric model discretization and velocity field

The problem model was discretized in 76 straight boundary elements (60 in Γ_1 and 16 in Γ_2) and 536 triangular cells, with 504 cells Ω_1 domain and 32 in Ω_2 domain, as shown in Fig. 11.

Fig. 12 illustrates the vector velocity field of the fluid in the Ω_1 domain.

Velocity field is clearly disturbed near the obstacle, with higher velocities between the obstacle and the top and bottom channel boundaries. Near the left and right sides of the obstacle the velocity is

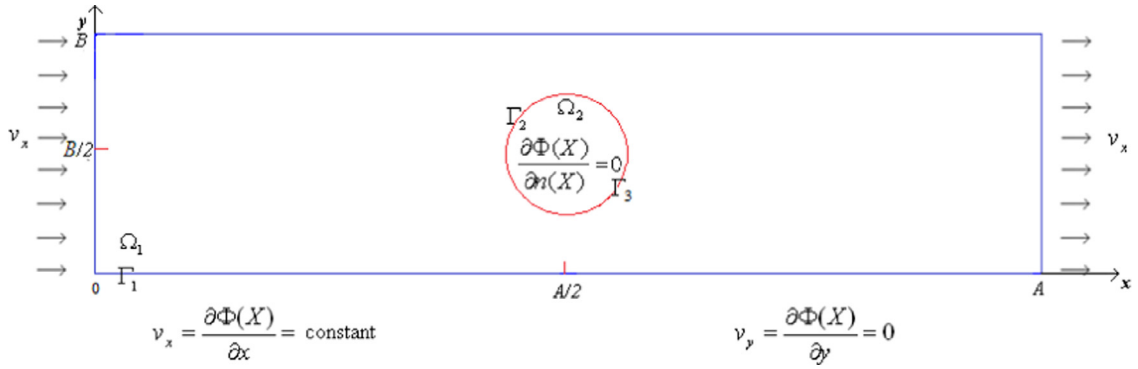

Fig. 10. Contour conditions of flow problem.

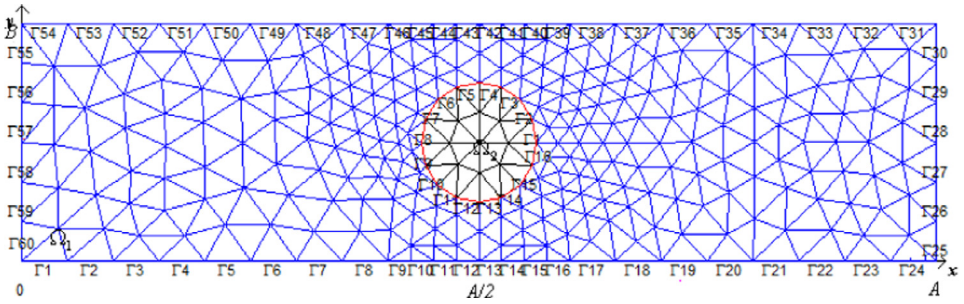

Fig. 11. Domain discretization.

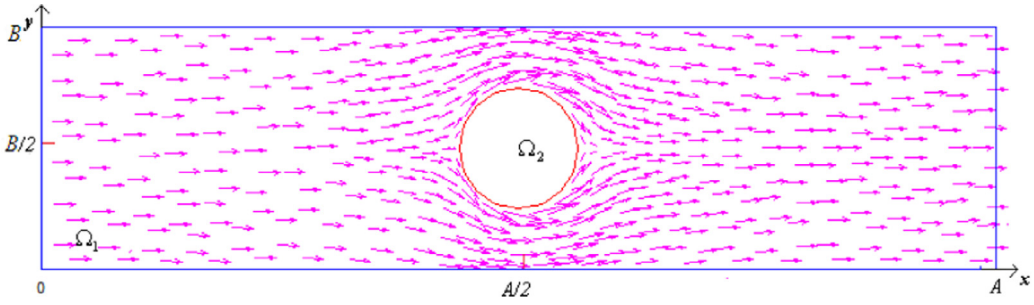

Fig. 12. Vector velocity field of the problem.

reduced approaching zero, corresponding to the expected stagnation points ($\theta = 0$ and $\theta = \pi$). A color velocity field (mm/s) map is shown in Fig. 13.

3.5.3. Problem conditions and results

The boundary and initial conditions for this analysis are:

$$u(X,t) = 0^{o}\text{C} \quad X \in \Gamma_1 \tag{47}$$

and

$$u_0(X,t_0) = 0^{o}\text{C} \quad X \in \Omega \tag{48}$$

respectively, representing constant and null temperature on the boundary along time and null initial temperature throughout the domain.

The heat source term in the obstacle domain Ω_2 is considered constant along time, given by:

$$\frac{F(X,t)}{k} = 10^{o}\text{C mm}^{-2} \quad X \in \Omega_2,\ 0 < t < \infty \tag{49}$$

The adopted thermal diffusivity values for domains Ω_1 and Ω_2 were $\alpha_1 = 0.7$ mm^2/s and $\alpha_2 = 4.5$ mm^2/s, respectively. The far field constant velocity was considered as $v_x = 0.001$ mm/s. To evaluate the numerical results seven fixed points were selected (A to G) as shown in Fig. 14. This selection considered their location symmetry with respect to the center of the obstacle in order to enhance temperature differences due to the single direction fluid flow.

Fig. 15 illustrates the temperature evolution in the four selected points of domain Ω_1. Points A and B are in the upstream direction while F and G are in the downstream direction. It can be seen that the temperature at points A and G have similar and lower evolution due to their distance from the obstacle and proximity to the null temperature boundary conditions. On the other hand, higher temperature evolution is detected at points B and F, which are very close to the heating obstacle. Higher temperatures at point F, compared to point B in any instant, indicates the downstream transport of the heat energy supplied by the obstacle.

A similar temperature evolution trend is observed at points C, D and E of domain Ω_2 (see Fig. 16). In this domain the heat is generated and transferred to the domain Ω_1 through their interface. The center point D is less influenced by the interface proximity and reaches higher temperature values. At points C and E, temperature rises similarly, but temperatures at E are slightly higher compared to temperatures in C, which is in agreement with the downstream heat energy transport.

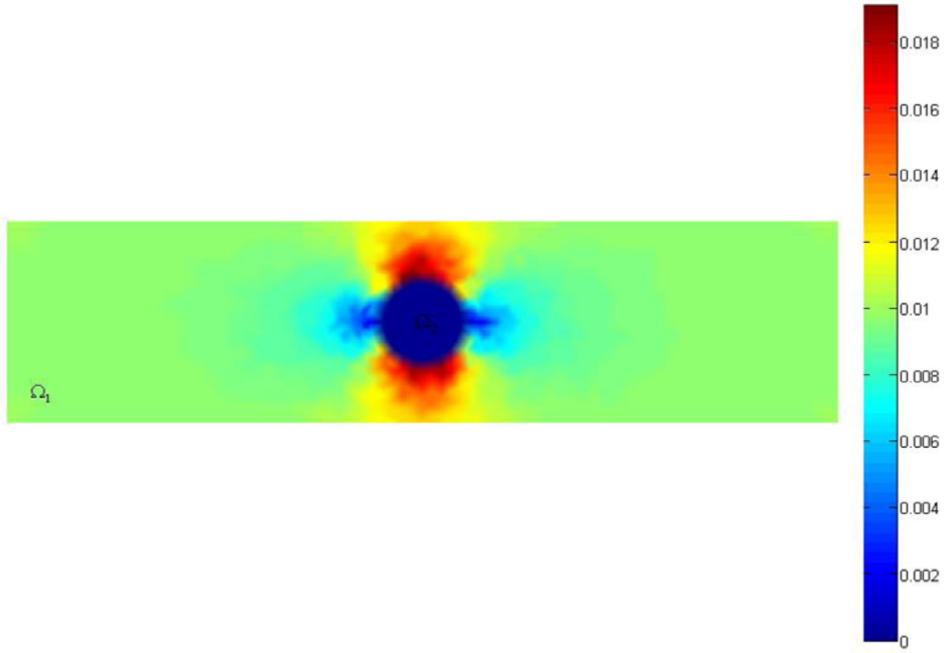

Fig. 13. Module of field velocity in the problem domain.

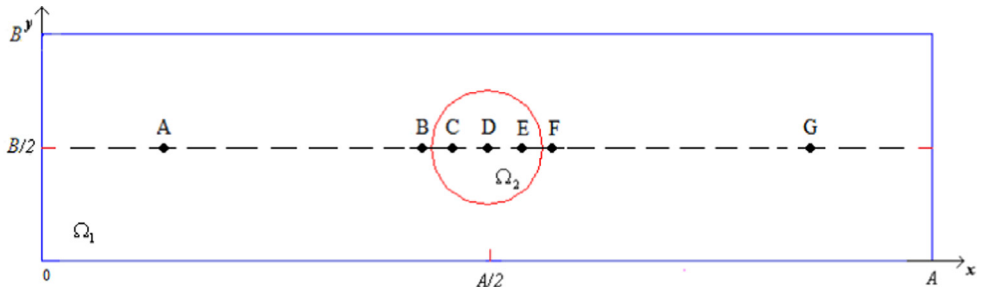

Fig. 14. Illustration of the location of the points analyzed.

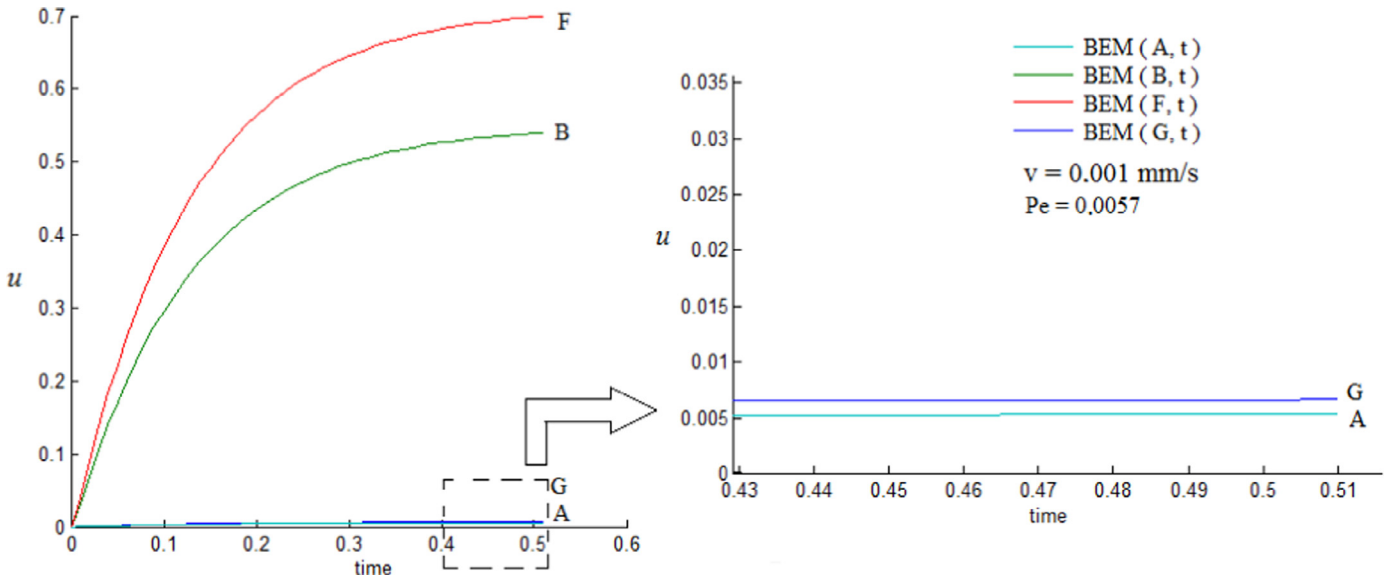

Fig. 15. D-BEM solutions for temperature distributions in A, B, F and G domain points.

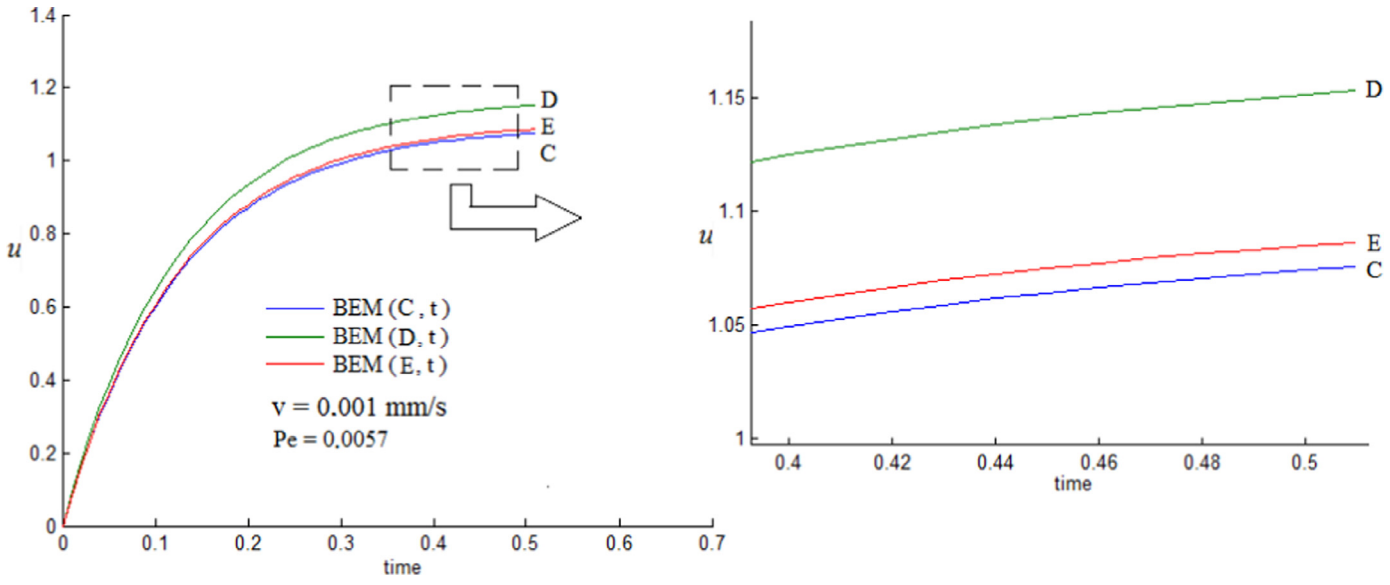

Fig. 16. D-BEM solutions for temperature distributions in C, D and E obstacle domain points.

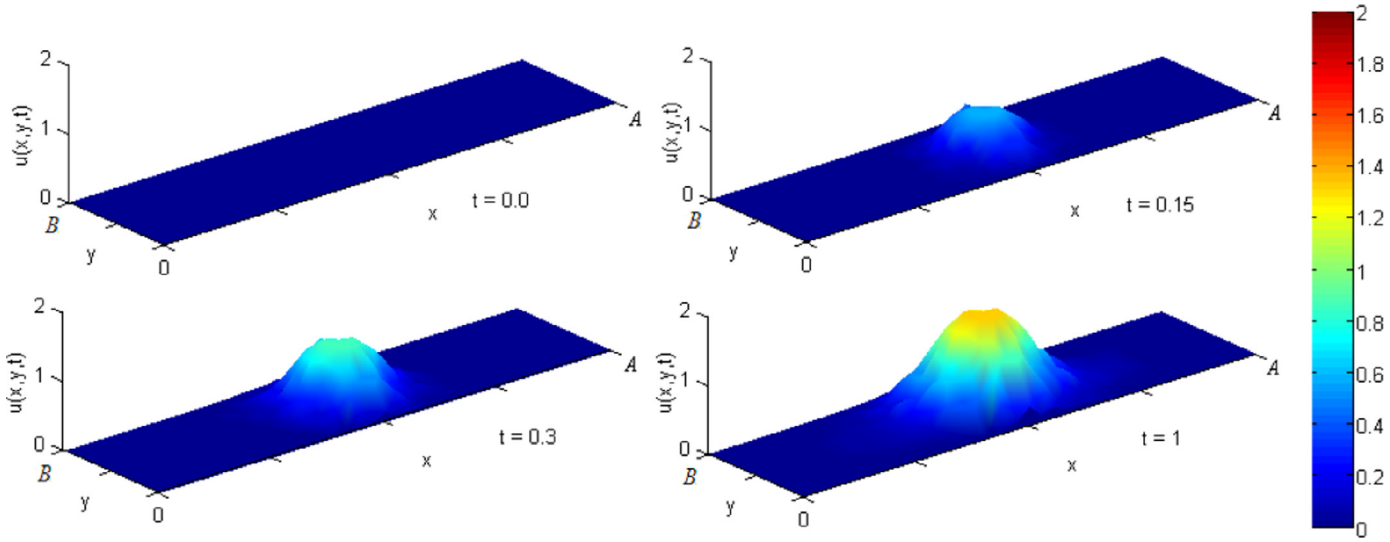

Fig. 17. Solution in the domain for different times on under heat generation at disk.

Fig. 17 illustrates the heat energy source generation inside the obstacle domain and its diffusion toward the advective domain along time. The advection heat transport is not clearly observed in this sequence since temperature differences are only noticed close to the obstacle boundary.

Temperatures along the longitudinal central section of the domain are plotted at time t = 0.52 s in Fig. 18. The lack of symmetry as result of the advective transport is only clearly noticed at the edges of the tails at each side, regions I and II. The downstream tail stretches little longer than the upstream tail, coherently. In the same image the purely diffusive temperature distribution result (zero velocity) is plotted with a dashed line, emphasizing the subtle differences due to the stream.

In other analysis, the temperature values of the disk center point D were compared using the velocity values equal to 0, 0.001, 0.01 to 0.1 mm/s. The results of this analysis are illustrated in Fig. 19.

In Fig. 19 it is possible to observe that even in domain 2, where only heat diffusion occurs, the effect of the flow velocity is also perceived. Lower temperatures were recorded at the center of the disk when larger velocity values were adopted.

4. Conclusions

D-BEM formulations were implemented to study heat diffusion–advection in isotropic media with homogeneous subregions and including heat generation sources. A time independent fundamental solution was employed and domain integrals were discretized with constant triangular cells. The first order time derivative in the formulations were approximated by a backward finite difference scheme.

Results from the numerical models were compared with analytical solutions showing very good correlation $R^2 > 0.99$ in two classical diffusion–advection equation analyses.

Interesting numerical results for the diffusion–advection problem were also obtained from a model containing a circular obstacle with a heat generation source. The source was symmetrically placed in the restricted domain forcing a non-uniform velocity field distribution, which was represented by an approximated analytical velocity field based on an infinite domain. This problem result showed the heat dissipation and transport around the circular obstacle toward the flow direction, demonstrating subtly the coherent advective effect on the diffusive process. In the same problem, it was observed that the temperature in the advective

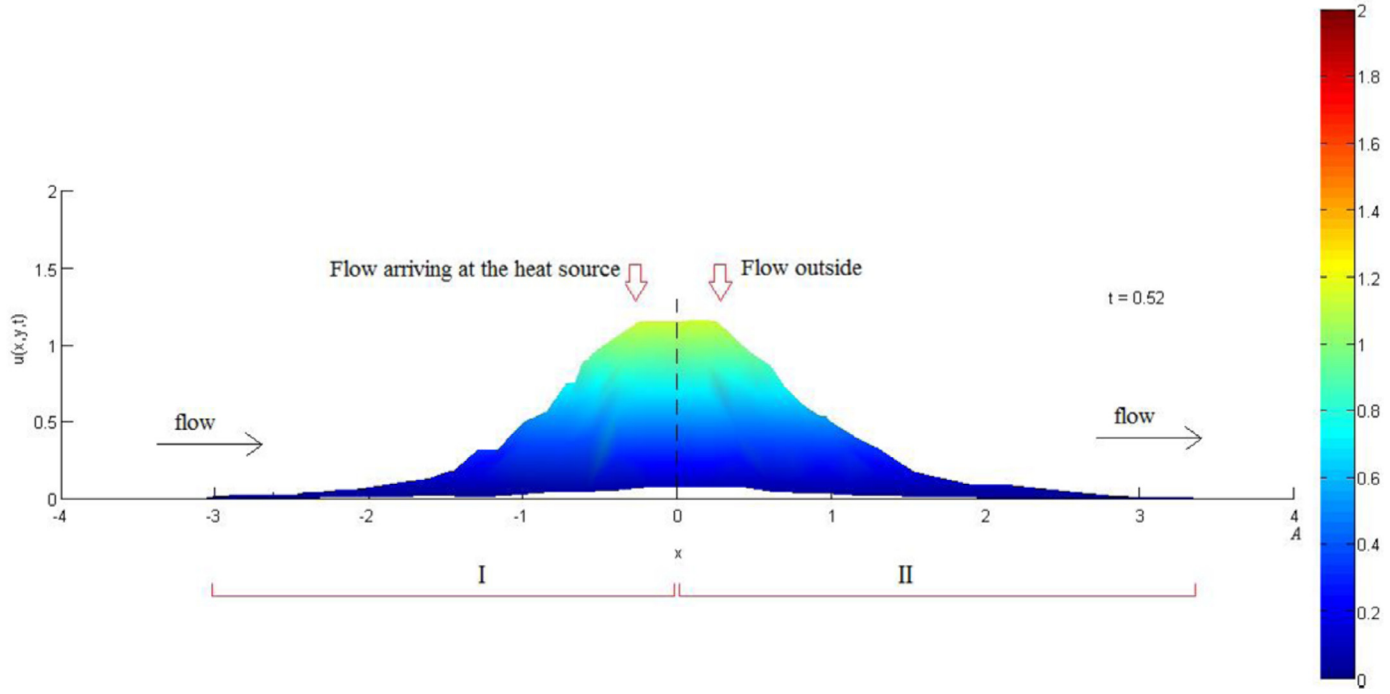

Fig. 18. Profile view of the numerical solution of the BEM for t = 0,52.

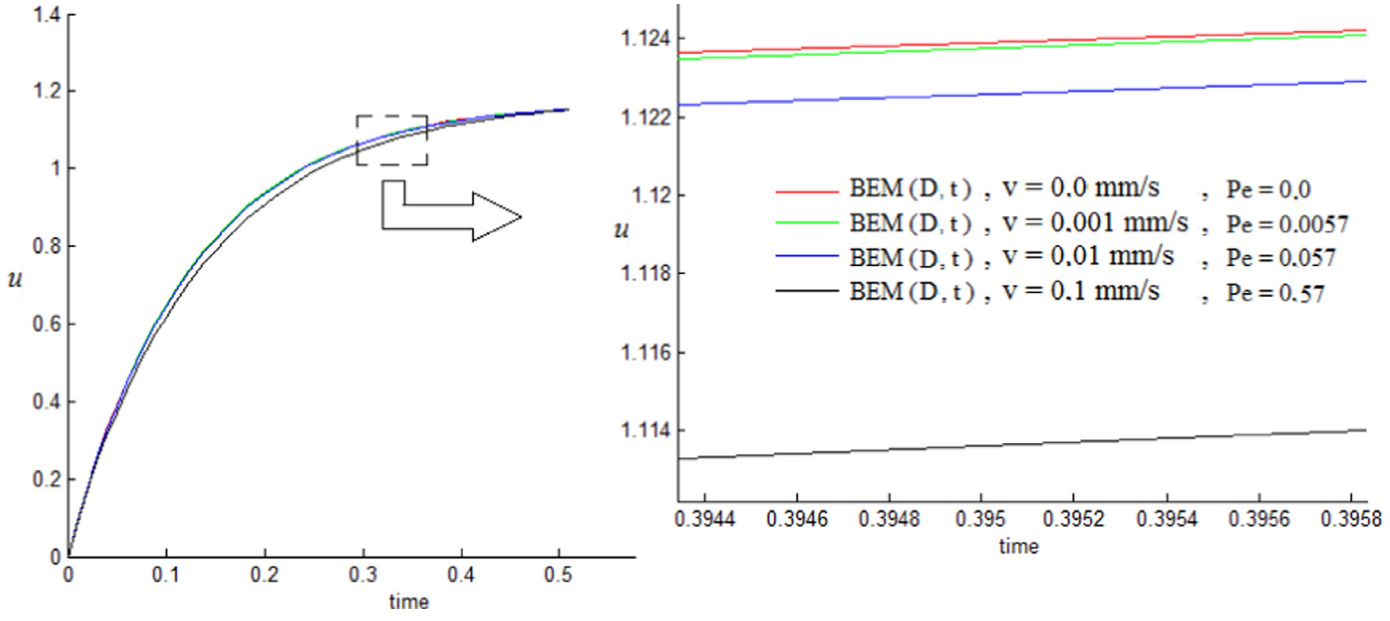

Fig. 19. BEM solutions for temperature distribution in the disk center to different flow velocity values.

domain near the source boundary showed great differences depending on the location, for the employed set of domain diffusive parameters and field velocity. And small differences were observed within the heat source near its boundary.

Despite the need for domain discretization, the results presented in the analyzed examples confirm the effectiveness of the D-BEM formulation for the evaluation of time-domain advective diffusion potential problems with internal heat sources.

Acknowledgments

The author would like to thank UFPR and INSTITUTOS LACTEC for the support for conducting this research.

References

[1] Brebbia CA, Dominguez J. Boundary elements an introduction course. Great Britain: Bath Press; 1989.
[2] Beer G, Watson JO. Introduction to finite and boundary element methods for engineers. England: Wiley; 1994.
[3] Wrobel LC. The boundary element method volume 1 applications in thermo-fluids and acoustic. England: John Wiley and Sons Ltd.; 2002.
[4] Spindler E. Second-kind single trace BEM for acoustic scattering. Symposium of the International Association for Boundary Element - IABEM 2013 Chile; 2013.
[5] Akalin-Acar Z, Gençer NG. An advanced boundary element method (BEM) implementation for the forward problem of electromagnetic source imaging, 49. Turkey: Physics in Medicine and Biology – Department of Electrical and Electronics Engineering Publishing, Middle East Technical University; 2004. p. 5011–28.
[6] Lacerda LA, Silva JM, Lázaris J. Dual boundary element formulation for half-space cathodic protection analysis. Eng Anal Boundary Elem 2007;31(6):559–67.

[7] Traub T. A Directional fast multipole method for elastodynamics. Symposium of the International Association for Boundary Element – IABEM 2013 Chile; 2013.
[8] Jesus JC, Azevedo JP. Computational simulation for 2D transition problems by the Contour Element Method using a fundamental solution independent of time. Centro Internacional de Métodos Computacionales en Ingeniería – Argentina, Mecánica Computacional Argentina; 2002.
[9] Vanzuit JR. Analysis of the two-dimensional heat flux by the contour element method with fundamental solutions independent of time. Curitiba: Federal University of Parana; 2007.
[10] Aurada MM, Feischl T, Führer M, Karkulik J, Melenk D. Convergence of adaptive FEM-BEM coupling driven by residual-based error estimators. 6th European Congress on Computational Methods in Applied Sciences and Engineering (ECCOMAS 2012) Vienna, Austria; 2012.
[11] Cheng AH-D, Cheng DT. Heritage and early history of the boundary element method. Eng Anal Boundary Elem 2005;29:268–302.
[12] Jesus JC, Pereira LL. Computational mathematical modeling by the contour element method for flow problems in porous media. XIII Congresso Brasileiro de Águas Subterrâneas; 2004.
[13] Brebbia CA, Skerget P. Diffusion-advection problems using boundary elements. Adv Water Resour 1984;7:50–7.
[14] Desilva SJ, Chan LC, Chandra A, Lim J. Boundary element method analysis for the transient conduction-convection in 2-D with spatially variable convective velocity. Appl Math Model 1998;22:81–112.
[15] Lima ETL Jr, Venturini WS, Benallal A. BEM modeling of saturated porous media susceptible to damage. Eng Anal Boundary Elem 2012;36(2):147–53.
[16] Young DL, Tsai CC, Murugesan K, Fan CM, Chen CW. Time dependent fundamental solutions for homogeneous diffusion problems. Eng Anal Boundary Elem 2004;28:1463–73.
[17] Azis MI, Clements DL. Nonlinear transient heat conduction problems for a class of inhomogeneous anisotropic materials by BEM. Eng Anal Boundary Elem 2008;32(12):1054–60.
[18] Abreu AI. A boundary integral formulation based on the convolution quadrature method for transient heat conduction in functionally graded materials. Symposium of the International Association for Boundary Element – IABEM 2013 Chile; 2013.
[19] Loeffler CF, Costalonga F. Hypersingular formulation of the contour elements method applied in diffusive-advective problems. X SIMMEC - Simpósio de Mecânica Computacional Belo Horizonte – MG Brasil; 2012.
[20] Ochiai Y. Two-dimensional unsteady heat conduction analysis with heat generation by triple-reciprocity BEM. Int J Numer Methods Eng 2001;51(2):143–57.
[21] Guo S, Zhang J, Li G, Zhou F. Three-dimensional transient heat conduction analysis by Laplace transformation and multiple reciprocity boundary face method. Eng Anal Boundary Elem 2013;37(1):15–22.
[22] Tanaka M, Kurokawa K, Matsumoto T. A time-stepping DRBEM for transient heat conduction in anisotropic solids. Eng Anal Boundary Elem 2008;32(12):1046–53.
[23] Singh KM, Tanaka M. Dual reciprocity boundary element analysis of transient advection-diffusion. Int J Numer Methods Heat Fluid Flow 2003;13:633–46.
[24] Sutradhar A, Paulino GH. The simple boundary element method for transient heat conduction in functionally graded materials. Comput Methods Appl Mech Eng 2004;193:4511–39.
[25] Stehfest H. Numerical inversion of Laplace transform. Commun Assoc Comput Mach 1970;13:19–47.
[26] Wei T, Zhang ZQ. Reconstruction of a time-dependent source term in a time-fractional diffusion equation. Eng Anal Boundary Elem 2013;37(1):23–31.
[27] Yu B, Yao W, Gao Q. A precise integration Boundary Element Method for solving transient heat conduction problems with variable thermal. Numer Heat Transf Part B 2014;65(5):472–93.
[28] Onishi K, Kuroki T, Tanaka M. An application of a Boundary Element Method to natural convection. Appl Math Model 1984;8:383–90.
[29] Greenberg MD. Application of Green's functions in science and engineering. New Jersey: Prentice-Hall; 1971.
[30] Morton KW, Mayers DF. Numerical solutions of partial differential equations. New York: Cambridge University Press; 1994.
[31] Wrobel LC. Potential and viscous flow problems using the boundary element method Ph.D. Thesis. U.K: University of Southampton; 1981.
[32] Pettres R, Lacerda LA, Carrer JAM. A boundary element formulation for the heat equation with dissipative and heat generation terms. Eng Anal Boundary Elem 2015;51(February):191–8.
[33] Sari M, Gürarslan G, Zeytinoğlu A. High-order finite difference schemes for solving the advection-diffusion equation. Math Comput Appl 2010;15(3):449–60.
[34] Rogers DF. Laminar flow analysis. Cambridge University Press; 1992.
[35] Çencel YA, Cimbala JM. Fluid mechanics–fundamentals and applications. São Paulo: McGrawHill; 2007.